Structure of *Alcaligenes faecalis* Nitrite Reductase and a Copper Site Mutant, M150E, That Contains Zinc[†,‡]

Michael E. P. Murphy,[§] Stewart Turley,[§] Mutsuko Kukimoto,[∥] Makoto Nishiyama,[⊥] Sueharu Horinouchi,[∥] Hiroshi Sasaki,[⊥] Masaru Tanokura,[⊥] and Elinor T. Adman*[,§]

Department of Biological Structure, Box 357420, School of Medicine, University of Washington, Seattle, Washington 98195-7420, and Department of Biotechnology, Faculty of Agriculture, and Biotechnology Research Center, The University of Tokyo, Yayoi 1-1-1, Bunkyo-ku, Tokyo 113, Japan

Received June 6, 1995; Revised Manuscript Received July 11, 1995[⊗]

ABSTRACT: The structures at 2.0 and 2.25 Å resolution of native and recombinant nitrite reductase from *Alcaligenes faecalis* show that they are identical to each other and very similar to nitrite reductase from *Achromobacter cycloclastes*. The crystallographic structure of a mutant, M150E, which unlike the wild-type protein cannot be reduced by pseudoazurin, shows that the glutamate replacement for methionine binds to a metal at the type I Cu site via only one oxygen. Anomalous scattering data collected at wavelengths of 1.040 and 1.377 Å reveal that the metal at the type I site is a Zn. No significant differences from the native structure other than local perturbations at the type I site are seen. A local pseudo 2-fold axis relates the two domains of different monomers which form the active site. The two residues, Asp98 and His255, believed to be involved in catalysis are related by this 2-fold. An unusual + − + charge interaction between Lys269, Glu279, and His100 helps to orient the active site Cu ligand, His100. A number of negatively charged surface residues create an electrostatic field whose shape suggests that it may serve to direct incoming negatively charged nitrite as well as to dock the electron donor partner, pseudoazurin.

Nitrite reductase from the denitrifying bacteria *Alcaligenes faecalis* strain S-6 is a copper-containing enzyme that converts nitrite to nitric oxide (NO_2^- to NO) under anaerobic conditions (Kakutani et al., 1981b). The *in vivo* electron donor has been shown to be a small blue copper protein, pseudoazurin (Kakutani et al., 1981a). When reduced by pseudoazurin, the enzyme produces H_2O_2 in the presence of O_2 and is inactivated. The enzyme is green, strongly inhibited by copper chelators, and contains both type I and type II copper sites as shown by EPR spectroscopy. The NIR[1] gene has been isolated and the protein expressed in the periplasm in *Escherichia coli* (Nishiyama et al., 1993). NIR is a functional trimer of 37 kDa subunits.

The sequence of mature *Af*NIR contains 343 amino acid residues and is 81% identical to the sequence of the copper-containing NIR from *Achromobacter cycloclastes* (Fenderson et al., 1991). An equivalent pseudoazurin has been isolated from this organism as well. The crystal structure of *Ac*NIR has been determined (Godden et al., 1991) and revealed a trimer with two Cu atoms per monomer. Each monomer is constructed from two β-barrel domains. The ligands of the type I site were identified as His95, Cys136, His145, and Met150. As is typically observed in type I sites, the histidine and the cysteine residues coordinate the copper in a distorted trigonal-planar geometry, and the methionine residue forms a weaker interaction in the axial position. The type II site is located at the interface between two monomers and is liganded by a solvent oxygen and three histidine residues, His100 and His135 from one subunit and His306 from another subunit.

On the basis of the sequence identity between the *A. faecalis* and *A. cycloclastes* enzymes, site-directed mutagenesis was used to probe the role of the copper atoms (Kukimoto et al., 1994). Mutation of His135[2] to lysine eliminated nitrite reductase function, indicating that the type II copper is the site of nitrite reduction. A mutation at the type I site, M150E, reduced the efficiency of electron transfer with pseudoazurin but left measurable nitrite-reducing activity using methyl viologen as the reductant, indicating that reducing electrons have to go through the type I Cu first. A bimolecular rate constant of 1.8×10^6 M^{-1} s^{-1} has been determined for the electron-transfer reaction between pseudoazurin and *Af*NIR using electrochemical techniques (Iwasaki et al., 1992). This study also showed that nitrite reduction is the rate-limiting step in the overall reaction.

Crystals of wild-type NIR from *A. faecalis* were originally produced from solutions of ammonium sulfate at pH 6.0 (Kakutani et al., 1981b) but were not used for data collection. A second crystal form was produced from PEG 4000 at pH

[†] This work is supported by NIH Grant GM31770 (to E.T.A.), an MRC of Canada Fellowship (to M.E.P.M.), a Grant-in-Aid from the Ministry of Education, Science and Culture of Japan (to M.N.), and a grant from the Japan Society for the Promotion of Science (to M.K.).

[‡] Coordinates for native and mutant *A. faecalis* NIR have been deposited in the Protein Data Bank (file names 2AFN and 1NTD).

* Author to whom correspondence should be addressed. Telephone: 206-543-6589. FAX: 206-543-1524. E-mail: adman@u.washington.edu.

[§] University of Washington.

[∥] Department of Biotechnology, Faculty of Agriculture, The University of Tokyo.

[⊥] Biotechnology Research Center, The University of Tokyo.

[⊗] Abstract published in *Advance ACS Abstracts,* September 1, 1995.

[1] Abbreviations: NIR, nitrite reductase; *Af*NIR, *Alcaligenes faecalis* NIR; *Ac*NIR, *Achromobacter cycloclastes* NIR; M150E *Af*NIR, a mutant of *Af*NIR where Met150 is replaced with glutamate; PEG, poly(ethylene glycol). Water molecules are assigned numbers by adding 1000 to the number of the nearest protein residue until a unique number is obtained.

[2] The amino acid numbering is that of *Ac*NIR based on the sequence alignment described in Nishiyama et al. (1993).

0006-2960/95/0434-12107$09.00/0

4.6−5.1 (Turley et al., 1988), and the structure was determined to 2.6 Å resolution (Kukimoto et al., 1994). The polypeptide fold is similar to that observed in *Ac*NIR with the same copper ligands.

Here we report the extension of the structure of wild-type NIR to 2.0 Å, the structure of the M150E mutant, and the recombinant form (to ensure that no differences seen in the mutant could be ascribed to differences due to the expression system). To see if the metal in the type I site of the M150E mutant was copper or zinc, we collected anomalous X-ray diffraction data at two wavelengths to distinguish between these two metals.

EXPERIMENTAL PROCEDURES

Protein Purification and Crystallization. Three different forms of NIR, native, recombinant, and a M150E mutant, were studied. Native NIR from *A. faecalis* was purified as described previously (Nishiyama et al., 1993). Recombinant NIR and the M150E mutant were expressed in *E. coli* and purified as described elsewhere (Kukimoto et al., 1994). Crystals of each form of NIR were obtained using the hanging drop method at room temperature under similar conditions as follows. Protein solutions were concentrated to about 10 mg/mL, and the buffer was exchanged with 10 mM MES, pH 6.0. Drops of protein solution were mixed with equal volumes of reservoir solution containing 10%−25% PEG 4000 and 0.1 M sodium acetate, pH range of 4.0−4.8. The $P2_1$ crystal form was observed for all three NIRs, whereas the $R3$ form has been observed only for the mutant and the orthorhombic form only for the native and recombinant enzymes. Initially, all crystals were grown in the presence of 1 mM sodium azide, used to prevent bacterial growth in stock PEG 4000 solutions. Crystals of the recombinant NIR were soaked in azide-free synthetic mother liquor prior to data collection to remove any azide bound to the protein. The wild-type and recombinant crystals were green while the M150E *Af*NIR crystals were a faint amber color.

Data Collection. A Rigaku R-AXIS IIc image plate system was used to collect X-ray diffraction data from the native and recombinant NIR crystals. Cu Kα radiation was produced from a rotating anode generator operated at 50 kV and 100 mA. The X-rays used to collect the native data set were passed through a graphite monochromator whereas focusing mirrors were in place when the recombinant data set was collected. The M150E *Af*NIR data were collected on a Siemens X1000 multiwire detector using copper radiation from a rotating anode generator at 50 kV and 80 mA with a graphite monochromator. The details of each data collection are summarized in Table 1. The lower completeness of the recombinant data set is due to the systematic absence of a cusp of data around the crystal rotation axis. Data collected on the R-AXIS were processed using software provided by the manufacturer (Higashi, 1990). The XENGEN package (Howard et al., 1987) was used to process data obtained from the Siemens instrument.

Data for anomalous scattering experiments were collected at the Photon Factory (Tsukuba, Japan) at beamline 6A. The first data set was collected with an oscillation angle of 7.5° and an exposure of 90 s per frame. The incident radiation of 1.3772 Å is immediately above the Cu anomalous scattering edge and below the Zn edge. A second data set was collected with an oscillation angle of 5° for 60 s per frame and λ = 1.0400 Å, which is above both the Cu and Zn K edges. One crystal of space group $P2_1$ aligned along the b^* axis was used for both data sets, translating the crystal between sets. The total X-ray exposure of the crystal was 75 min. Two image plates placed in a 286.5 mm radius Weissenberg camera were used for each frame. The frames were indexed and integrated with the program WEIS, and the resulting intensities were scaled and merged with the programs ROTAVATA and AGROVATA (Collaborative Computational Project, Number 4, 1994). Additional data collection statistics are presented in Table 1. During data processing we noticed that the upper plates which were scanned on a different scanner than the lower plates resulted in significantly higher resolution data.

Table 1: Data Collection Statistics of *Af*NIR and the M150E Mutant and Anomalous Scattering Data for M150E *Af*NIR

(a) Data Collection Statistics of *Af*NIR and the M150E Mutant

crystal	native	recombinant	M150E
space group	$P2_12_12_1$	$P2_12_12_1$	$R3$
cell dimensions (Å)	a = 63.04, b = 103.61, c = 146.90	a = 63.30, b = 103.43, c = 147.30	$a = b$ = 127.76, c = 67.02
resolution (Å)	2.0 (2.25−2.0)[a]	2.25 (2.5−2.25)	2.3 (2.5−2.3)
R_{merge}[b] on I	0.051 (0.154)	0.045 (0.124)	0.061 (0.199)
$\langle I\rangle/\langle\sigma(I)\rangle$	14.6 (4.3)	14.7 (4.0)	15.9 (5.1)
completeness	0.85 (0.69)	0.76 (0.54)	0.93 (0.90)
unique reflections	55751 (13333)	35769 (6656)	17281 (4167)
redundancy	3.2 (2.3)	2.4 (1.6)	2.0 (1.6)

(b) Anomalous Scattering Data for M150E *Af*NIR

	wavelength (Å)	
	1.0400	1.3772
space group	$P2_1$	
cell dimensions	a = 73.75 Å, b = 93.11 Å, c = 78.63 Å, β = 96.06°	
resolution (Å)	2.3 (2.4−2.3)[a]	2.4 (2.5−2.4)
R_{merge} on I	0.054 (0.229)	0.075 (0.215)
$R_{anomalous}$[c] on I	0.051 (0.158)	0.056 (0.149)
$\langle I\rangle/\langle\sigma(I)\rangle$	10.0 (2.4)	7.5 (3.0)
completeness	0.77 (0.67)	0.92 (0.83)
unique reflections	36170 (4501)	38095 (4985)
redundancy	2.6 (1.9)	2.8 (2.5)

[a] Values in parentheses are for the highest resolution shell. [b] $R_{merge} = \sum_{hkl}\sum_{i=1}^{n}|I_i(hkl) - \langle I(hkl)\rangle|/\sum_{hkl}\sum_{i=1}^{n}I_i(hkl)$. [c] $R_{anomalous} = \sum_{hkl}|I(hkl) - I(\overline{hkl})|/\sum_{hkl}|I(hkl) + I(\overline{hkl})|$.

Structure Solution and Refinement. The native and recombinant crystals are isomorphous with the native crystal used to determine the structure to 2.6 Å resolution (Kukimoto et al., 1994) and contain the entire NIR trimer in the asymmetric unit. This structure was used as the starting point for refinement against native NIR data to 2.0 Å resolution [$F > 3\sigma(F)$]. A randomly selected portion (8%) of the data was reserved for computation of the free R-factor (Brünger, 1992). The starting conventional and free R-factors were 0.307 and 0.309, respectively. Refinement was carried out with the program X-PLOR (Brünger, 1990) using the parameter set parhcsdx.pro (Engh & Huber, 1991). The copper geometry was not restrained except for the copper oxygen distance of the type II site water ligand, which was moderately restrained to 2.0 Å (bond energy constant of 100 kcal mol^{-1} Å^{-2}). B-factors were refined using the same resolution range (Table 2) for 25−40 steps per refinement cycle. The program PROCHECK (Laskowski et al., 1993) was used to identify regions of the molecule requiring manual

Table 2: Refinement Statistics of *Af*NIR and the M150E Mutant

parameter	native	recombinant	M150E
resolution range (Å)	10−2.0	10−2.25	10−2.3
working *R*-factor	0.158	0.159	0.172
free *R*-factor	0.223	0.227	0.232
rms deviation from ideal geometry			
bond length (Å)	0.009	0.010	0.011
bond angles (deg)	1.72	1.71	1.87
improper torsions (deg)	1.38	1.42	1.55
overall *B*-factor (Å^2)	24.7	28.2	21.7
av *B*-factor of solvent (Å^2)	35.7	35.7	30.2
B-factor range for type 1 metal (Å^2)	18.1−24.7	19.3−27.1	19.5
B-factor range for type 2 metal (Å^2)	20.7−26.0	23.0−29.8	16.3
no. of reflections	48320 (0.74)[a]	30601 (0.65)	13011 (0.70)
no. of protein atoms	7596	7596	2566
no. of solvent atoms	477	324	92

[a] The values in parentheses are the percent completeness of the data used in refinement.

adjustment, which was done using the program O (Jones et al., 1991). Solvent molecules were identified by searching for peaks in $F_o - F_c$ maps using the CCP4 suite of programs (Collaborative Computational Project, Number 4, 1994). Final refinement statistics are given in Table 2. The first eight residues and the last residue of each monomer are disordered and are not present in the final model. The overall *B*-factors for subunits A, B, and C are 21.5, 24.0, and 26.6 Å^2, respectively. The difference in these *B*-factors may be due to differences in crystal packing for each subunit.

Intensities from recombinant NIR were scaled against the native data set to 2.25 Å, and the resulting *R*-factor between data sets on *F* was 0.166. The final refined structure of native NIR was used to provide phases for a $F_o^{native} - F_o^{recombinant}$ difference map which showed no significant differences. The initial *R*-factor and free *R*-factor were 0.267 and 0.263, respectively, and the structure was refined as described above. The same residues as in the native structure are included in the final structure. Final refinement statistics are given in Table 2.

The M150E *Af*NIR crystals are of the space group *R*3 with the trimer 3-fold axis coincident with the crystallographic 3-fold axis. This results in the asymmetric unit containing only one monomer. Molecular replacement, using the program AMORE (Navaza, 1994), provided the orientation of the molecule in the new cell. The search model was subunit A of the final refined structure of native NIR with coordinates of the Met150 side chain and the solvent atoms removed. An unambiguous rotation solution was obtained using data from 20 to 3 Å resolution and a sphere radius of 29 Å. Data from 8 to 3 Å were used to obtain the translation solution. After rigid body refinement the conventional *R*-factor was reduced to 0.27 against data from 20 to 3 Å resolution.

The structure was refined using the same techniques described for native NIR. An $F_o - F_c$ difference map was used to fit in the Met150 side chain with residue 150 omitted from F_c. The starting *R*-factor and free *R*-factor were 0.256 and 0.264, respectively (data from 8 to 2.5 Å resolution). In the final structure, the first four residues are disordered and are not included in the model. The final refinement statistics are also reported in Table 2.

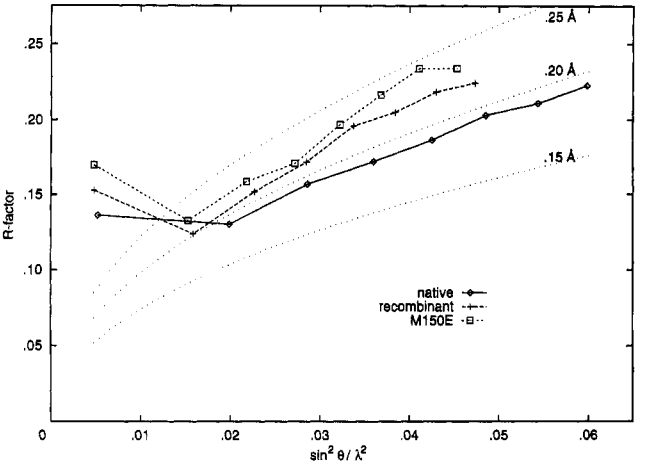

FIGURE 1: A plot of *R*-factor versus $\sin^2 \theta/\lambda^2$ for native, recombinant, and M150E *Af*NIR. The dotted lines are expected *R*-values computed by assuming varying coordinate errors (Luzzati, 1952).

The final refined M150E *Af*NIR trimer was used for the molecular replacement solution of the monoclinic crystal form. An unambiguous initial orientation was found and refined using AMORE and the data set collected with 1.0400 Å radiation. One round of positional and *B* refinement with X-PLOR against 29 260 reflections reduced the conventional and free *R*-factors from 0.265 and 0.266 to 0.195 and 0.253, respectively. This partially refined model was used to provide phases for anomalous difference maps computed at both wavelengths. The use of anomalous scattering at two wavelengths to distinguish between two metals of similar atomic number has been described previously (Einspahr et al., 1985).

RESULTS

Structure Reliability. The rms error in the coordinates is estimated to be 0.2 Å by the method of Luzzati (Figure 1). After least squares superposition, the average difference of main-chain atom positions between the subunits in the native trimer is 0.18 Å. One segment of chain comprising the majority of the C-terminal β-barrel (residues 230−335) and the C-terminal extension contains no large external loops. The average main-chain difference in this region is lower (0.12 Å). Several other smaller segments of polypeptide chain in the amino-terminal domain possess significantly different coordinates (average deviation greater than 0.5 Å) between subunits. All of these regions are external loops and are either disordered or are involved in crystal contacts. The main chain of residues 33, 34, 165−168, and 188−191 of each subunit in all three structures is disordered, and the model at these positions is not reliable (Figure 2). This disorder is reflected in the crystallographic *B*-factors which are greater than 50 Å^2.

Polypeptide Fold. Each of the three identical subunits contains two Cu atoms and a 343 amino acid polypeptide chain (Figure 3). Two Greek key β-barrel domains form the bulk of each subunit. The N-terminal domain (residues −3 to 160) interacts with two carboxy-terminal domains (residues 171−340), one from the same subunit and one from an adjacent subunit in the trimer. Each C-terminal domain interacts with two amino-terminal domains and two other C-terminal domains near the 3-fold axis. Residues 161−170 link the two domains, and residues 321−340 are in an

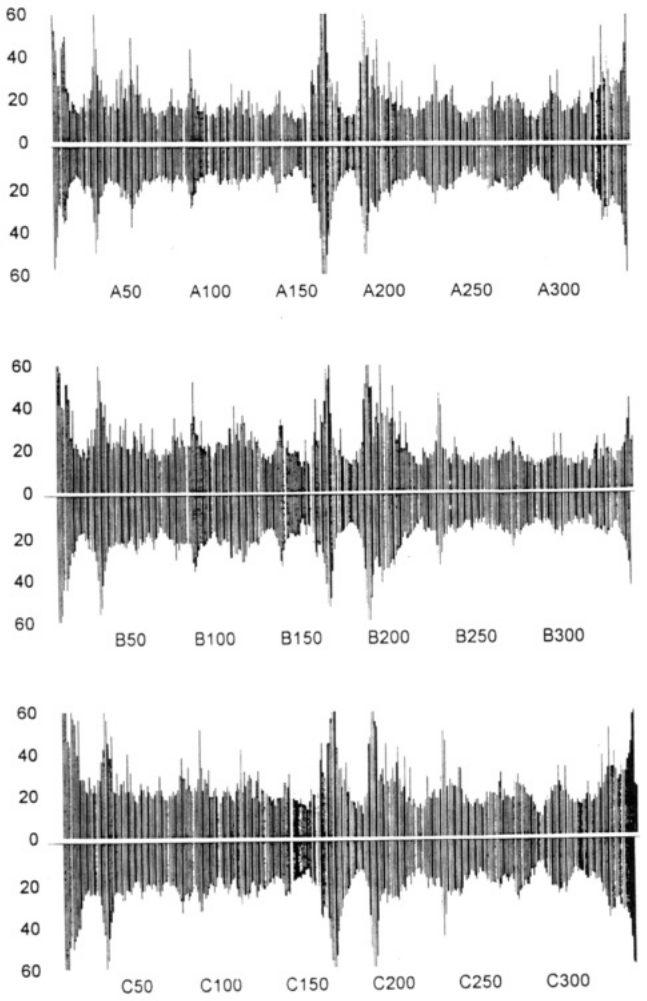

FIGURE 2: Average crystallographic *B*-factors as a function of residue number of the three subunits of *Af*NIR. The main-chain values are above the axes; the side-chain values are below. The horizontal axes are labeled by the residue number and chain identification letter for each subunit.

extended conformation and interact only with the N- terminal domain of different subunits.

The surface areas buried by each of these domain−domain interactions are presented in Table 3. A total molecular surface area of about 12 000 Å^2 is buried upon formation of the NIR trimer from three monomers. The interface between the monomers is 57% hydrophobic and contains many intersubunit hydrogen bonds and salt bridges. These polar interactions are especially evident at the interface between C-terminal domains near the 3-fold axis. The C-terminal tail accounts for approximately half of the buried surface between the N- and C-terminal domains from adjacent subunits. Approximately 4000 Å^2 of surface is buried upon joining the two domains of a subunit. The interface between the two domains of a subunit is more hydrophobic (68%) than the monomer−monomer interface. The monomers are constructed primarily of β-sheets; however, three segments of α-helix are also present. One of these helices, residues 307−315, interacts with the remaining two helices, residues 141−149 and 202−213. These interactions occur between residues from different monomers, stabilizing the trimer, and include residues that form the pocket containing the type II Cu site.

A channel is present along the 3-fold axis of the trimer (Figure 4). This channel is occluded near its midpoint by

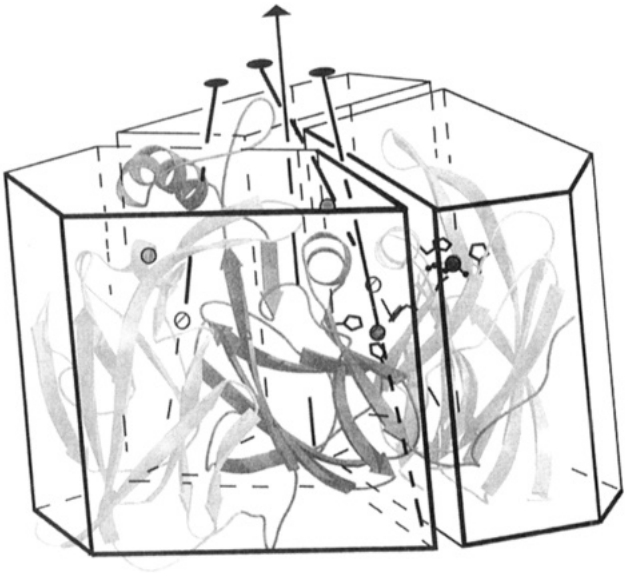

FIGURE 3: Schematic diagram of the trimer of nitrite reductase showing the 3-fold axis and the pseudo-2-fold axes. A ribbon diagram of two domains from one subunit and another domain from an adjacent subunit of *Af*NIR is superimposed on the diagram showing the position of the Cu atoms. This figure and Figures 4 and 6 were created with MOLSCRIPT (Kraulis, 1991) and RASTER3D (Merritt & Murphy, 1994).

Table 3: Domain Solvent-Accessible Surface Area Buried upon Subunit and Trimer Formation (Å^2)[a]

	subunit formation		trimer formation	
domain	N-terminal	C-terminal	N-terminal	C-terminal
N-terminal		2030 (69)		1200 (60)
C-terminal	1940 (67)		1340 (63)	790 (53)
				720 (48)[b]

[a] Each value is an average of the surface buried for the same domain of each subunit. The number in parentheses is the percentage of the buried surface that is hydrophobic. Surface areas were calculated using a probe size of 1.4 Å and removing the coordinates of each domain of the trimer individually (Connolly, 1983). [b] Each C-terminal domain contacts two other C-terminal domains.

Phe282. The phenyl ring planes are arranged at 20° to the 3-fold axis and interact with each other at the ring edges. Stacked immediately above the phenyl groups is a ring of salt bridges formed by Asp251 and Arg253 from a symmetry-related subunit. Similarly, Arg250 and Glu310 form a second wider ring of three salt bridges above Asp251 and Arg253. Both residues are provided by the same subunit. The presence of these four residues creates a highly charged section of the trimer channel. The channel then narrows and is lined by the side chain of Thr214 and the main chain of Ala271. The channel immediately on the other side of Phe282 is formed by Thr267 and Ala266, which do not form specific interactions. Bound water molecules are observed throughout this channel except for a 4 Å thick section of the molecule at Phe282.

A search for cavities using the program VOIDOO was undertaken (Kleywegt & Jones, 1994). In addition to the trimer channel and the active site pocket, a large buried cavity (probe accessible volume of ~35 Å^3) is found within each of the subunits. The cavity is lined by 17 residues of which Val59, His60, Trp144, Tyr184, Val185, Tyr196, and Pro199 are the most prominent and contains eight crystallographically observed solvent molecules. The channel extends from disordered residues at the molecular surface to Trp144, which

FIGURE 4: View of the central core of the channel with the trimer axis perpendicular to the page. The side chains are drawn as sticks and are labeled. Sections of polypeptide backbone are represented as coil, sheet, and helix.

is adjacent to His145, a type I site ligand. The proximity of the cavity to the type I site suggests that it may have a functional role.

Structure of the Type II Copper Site. The type II Cu site is located at the bottom of a 14 Å deep pocket formed at the interface between the N- and C-terminal domains from two different subunits. Two of the histidine ligands (His100 and His135) are provided by the N-terminal domain of one subunit, and the third ligand (His306) originates from the C-terminal domain of another subunit. An oxygen atom (water 503) was used to model a water or hydroxyl group as the fourth ligand. Additional difference density is observed surrounding this fourth ligand in the native structure (Figure 5). Both azide and acetate are present in the crystallization medium and may ligand to the Cu at partial occupancy; however, these ligands could not be convincingly modeled into this density. The *B*-factors of the copper atoms of each type II site (Table 2) are greater than the average *B*-factors of the corresponding ligands, suggesting that the metal sites are less than fully occupied.

All three histidine ligands interact with the Cu atom via the Nϵ2 atoms of the imidazole rings and are arranged in a distorted tetrahedral arrangement (Table 4). These histidine ligands also form hydrogen bonds via the Nδ1 atoms. His135 and His306 are hydrogen bonded to the main-chain carbonyls of Cys136 and Ala248, respectively. The main chain of residues 302−307 is distorted from ideal geometry as observed in the *Ac*NIR structure (Adman et al., 1995). The carboxyl group of Glu279 is hydrogen bonded to His100 Nδ1 and Lys269 Nζ as well as the main-chain amides of Val133 and Ala288. Residue 279 is located on a different subunit than the hydrogen bond partners. The histidine side chains liganded to the Cu have side-chain torsional angles near local minima.

His255 and Asp98 are two polar side chains located close to the Cu oxygen ligand and form part of the active site pocket. A water molecule (water 1098) is hydrogen bonded to the side chain of Asp98 and to the Cu oxygen ligand. This water initiates an extended network of hydrogen bonds

Table 4: Metal−Ligand Geometry of *Af*NIR and the M150E Mutant[a]

parameter	native	recombinant	M150E
(I) type I copper site (CuA)			
(a) ligand bond length (Å)			
95Nδ1	2.11	2.08	2.02
136Sγ	2.11	2.13	2.22
145Nδ1	1.97	1.88	2.04
150Sδ(Oϵ1)	2.63	2.63	1.98
150Oϵ2			2.81
(b) ligand bond angles (deg)			
95Nδ1−Cu−136Sγ	133	130	123
95Nδ1−Cu−145Nδ1	98	97	96
136Sγ−Cu−145Nδ1	107	110	107
136Sγ−Cu−150Sδ(Oϵ1)	104	104	113
150Sδ(Oϵ1)−Cu−145Nδ1	129	126	106
150Sδ(Oϵ1)−Cu−95Nδ1	89	91	108
(II) type II copper site (CuB)			
(a) ligand bond length (Å)			
100Nϵ2	2.02	2.03	2.00
135Nϵ2	2.13	2.11	2.28
306Nϵ2	2.16	2.15	2.23
503O	2.15	1.98	2.15
(b) ligand bond angles (deg)			
100Nϵ2−Cu−135Nϵ2	99	101	106
100Nϵ2−Cu−306Nϵ2	101	105	96
135Nϵ2−Cu−306Nϵ2	114	112	114
100Nϵ2−Cu−503O	151	144	152
135Nϵ2−Cu−503O	97	99	88
306Nϵ2−Cu−503O	95	93	100

[a] The bond lengths and angles for the native and recombinant structures are the average of three values. The average deviation of the individual bond lengths, excluding the water ligand, from the average was 0.06 Å for both these structures. Similarly, the bond average bond angle deviation was 2° for both structures. The errors in the M150E structure are expected to be higher.

formed by water molecules 1102 and 1100 to connect the active site residues to His260 Nϵ2 which lies in a depression at the molecular surface. The carbonyl of the His100 ligand is hydrogen bonded to both water 1100 and His260 Nϵ2. The Nδ1 atom of His260 is hydrogen bonded to water 1103 to provide the last link to bulk solvent. This chain of hydrogen bonds provides an alternate route for protons to the active site than the large active site pocket.

The deep pocket that directly connects the type II site to the surface is mostly lined with hydrophobic residues. Two large hydrophobic residues, Leu308 and Ile257, are within 6 Å of the Cu oxygen ligand, creating a hydrophobic pocket surrounding residues His255 and Asp98. There is a line of polar atoms provided by the main-chain carbonyls of residues 106, 109, and 137 and the side chains of Asn96 which connects Asp98 to Glu113, which is located at the mouth of the pocket. Notably, all of these polar atoms are on one side of the pocket. The type II Cu atom is 17 Å from the trimer axis at the center of the molecule near Phe282. There does not appear to be any direct access to the type II site from the trimer channel.

Structure of the Type I Site. The four ligands of the type I site are provided by the N-terminal domain of a single subunit. The Cu is liganded by the side chains of two histidine residues (His95 and His145), Cys136, and Met150. Similar to the type II site, the four ligands are arranged in a distorted tetrahedral arrangement (Table 4). In contrast to the type II site, the two histidines are liganded via the Nδ1 atoms. The side-chain torsional angles are near commonly observed values except for the χ_2 torsion angle of His145, which is −128°. As observed for the type II site, the average

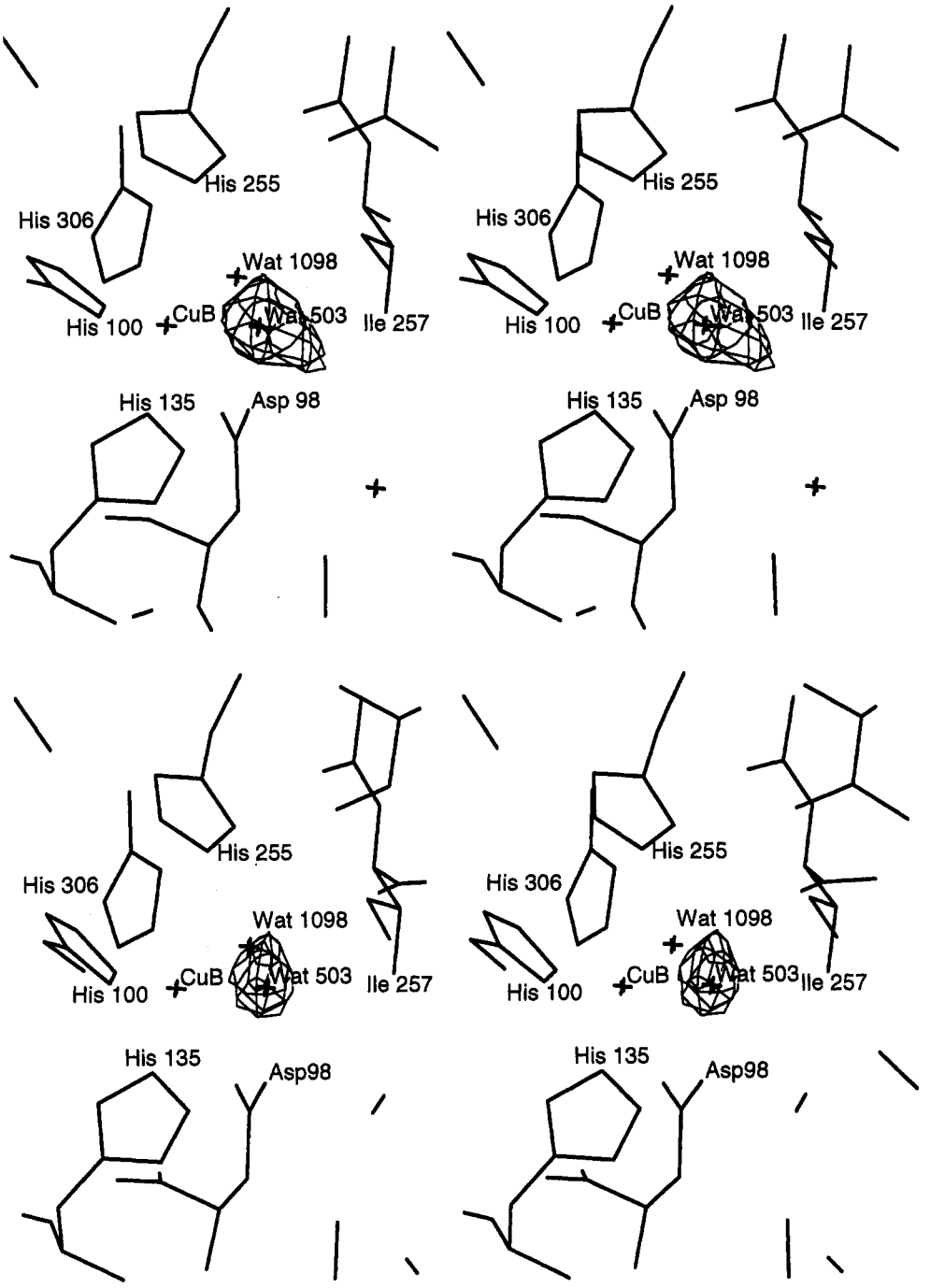

FIGURE 5: The type II site of native (top) and recombinant (bottom) *Af*NIR. $F_o - F_c$ maps with water 503 omitted from the structure factor calculation are contoured at 2.5σ. Unidentified density surrounding the water ligand in the native structure may be due to azide in the crystallization buffer.

crystallographic *B*-factors of the ligands are less than those of the type I site copper atoms (Table 2).

Residues His135 and Cys136 are liganded to the type II and type I Cu sites, respectively, and provide a direct covalent link between the two sites, which are 12.5 Å apart. The type I site is located closer to the top of the molecule (8 Å from the center) and more distant from the trimer axis (25 Å) than the type II site (in the orientation shown in Figure 4). The type I Cu is completely buried in the molecular interior, and His145 is the only Cu ligand near the molecular surface. The edge of the imidazole ring is at the bottom of a depression on the surface and is immediately surrounded by a hydrophobic patch formed by residues Leu93, Met94, Pro138, Pro139, Met141, Trp144, and Tyr203. Surrounding this hydrophobic patch is a ring of six negatively charged glutamate residues (113, 118, 197, 201, 204, and 313). This ring includes a residue from another subunit (Glu313) and one residue (Glu113) located at the entrance of the channel to the type II site.

Structure of Recombinant NIR. The recombinant form of NIR is essentially identical to that of wild-type NIR. The average deviation between main-chain atoms is 0.12 Å. Crystals of recombinant NIR were soaked in an azide-free medium prior to data collection and display less extraneous difference density than observed in the wild-type structure (Figure 5).

Structure of M150E AfNIR. The overall fold of the M150E mutant of NIR is similar to that of the wild-type protein

(average deviation of main-chain atoms of 0.23 Å). Some of the disordered loops are in alternate conformations due to different crystal contacts. The type II site geometry is not significantly affected by the mutation at the type I site (Table 4).

Like the Met150 side chain in the wild-type structure, the Glu150 side chain is a type I site metal ligand. Both of the side-chain carboxylate oxygens of Glu150 interact with the metal (Table 4); however, only the Oϵ1 atom is close enough to the metal to be considered a ligand. The Oϵ2 copper distance is similar to the Gly45 carbonyl copper distance observed in the azurin structure (Baker, 1988). The side chain of Glu150 is in a similar conformation to the side chain of Met150 such that Cδ (Glu) is 0.35 Å from Sδ (Met), and Oϵ2 (Glu) is 0.73 Å from Cϵ (Met). As a result, the Oϵ1 atom is 1.98 Å from the metal.

Metal−carboxylate interactions in proteins have been examined by comparing the orientation of the metal with respect to the carboxylate plane (Chakrabarti, 1990). Two angles are defined by placing the Cδ−Oϵ1 bond along the *x* axis with the Oϵ1 atom at the origin and Oϵ2 atom in the *xy* plane. The acute angle between the metal Oϵ1 bond and the *z* axis is defined as θ, and ϕ, is the angle between the projection of the Oϵ1 metal vector on the *xy* plane and the *x* axis. For Glu150 in M150E *AfNIR* the angles θ and ϕ are both 68°. These angles are within the range observed for other glutamate−metal ligands (Chakrabarti, 1990).

Two residues, Ile45 and Phe64, are displaced by the M150E substitution. Both of these residues pack against the Met150 side chain in wild-type NIR. The average side-chain displacements of 0.72 and 0.57 Å for Ile45 and Phe64, respectively, allow the introduction of the glutamate side chain which possesses an additional atom and a shape different from a methionine. The main-chain atoms of residues 63−66 are also displaced by ~0.5 Å by this mutation. No residues are observed to be within hydrogen-bonding distance of either carboxylate oxygen atom of Glu150, and no solvent lies in this region.

Density for a fully occupied metal is observed at the type I site. A Cu atom was used to model the density in the present refinement. The crystallographic *B*-factor for the type I site metal (19.5 Å^2) is within the range of values observed in the wild-type and recombinant NIR structures (Table 2). The type of metal cannot be unambiguously determined from the peak height of the electron density map but can be determined from anomalous scattering data collected at two wavelengths. Metals are strong anomalous scatterers when using incident radiation with a wavelength slightly shorter than an X-ray absorption edge. Anomalous scattering is detectable by measuring intensities for both F_{hkl} and $F_{\overline{hkl}}$ which would be equal in the absence of this effect. The K absorption edges of the transition metals of interest, Mn, Fe, Ni, Cu, and Zn, are 1.896, 1.743, 1.488, 1.381, and 1.284 Å, respectively. A wavelength of 1.3772 Å thus is slightly shorter than the anomalous scattering edge of Cu but below the edge for Zn so one would expect to see anomalous differences for Cu but not Zn. At 1.040 Å one would expect to see similar anomalous signal for both metals (Table 5). Thus, the small peak observed at the type I site in an anomalous scattering difference map computed using data collected at λ = 1.3772 Å shows that no significant Mn, Fe, Ni, or Cu is present at this site in M150E *Af*NIR (Figure 6). The appearance of a large peak when the wavelength is shifted to 1.040 Å is consistent with the presence of a Zn atom in this type I site. Other metals with anomalous scattering edges between 1.37 and 1.04 Å can be eliminated since they are not present in sufficient quantity in the growth media or subsequent purification buffers. These metals include Ge, Ga, As, and a series of the lanthanides.

Table 5: Anomalous Scattering Factors in Electrons for Cu and Zn at the Two Wavelengths Used in Data Collection

wave-length (Å)	f' (e$^-$)		f'' (e$^-$)	
	Cu	Zn	Cu	Zn
1.377	−5.63	−2.40	3.88	0.54
1.040	−2.50	−0.56	2.44	2.73

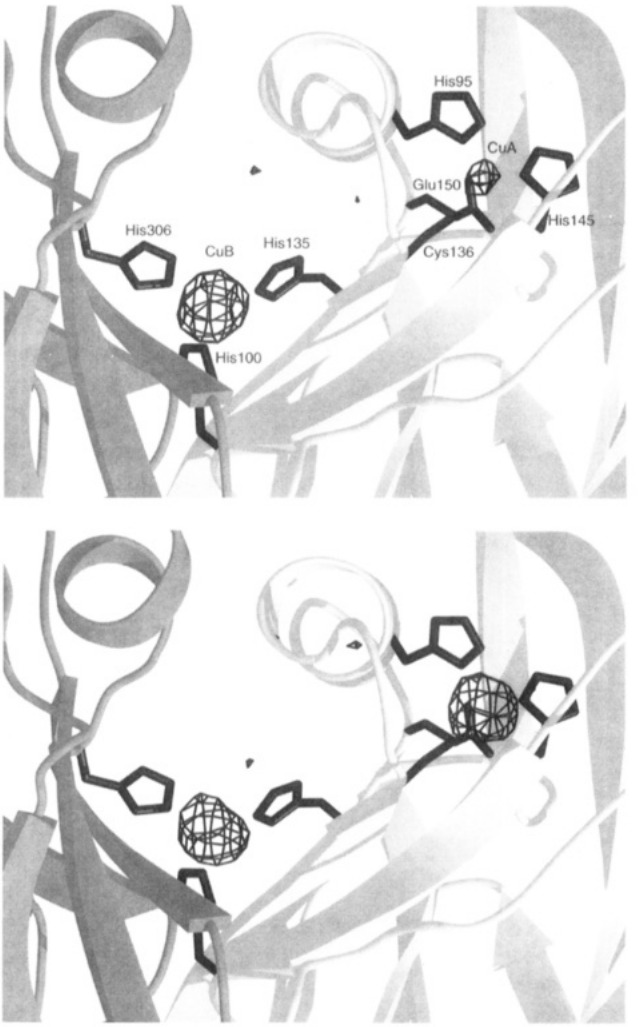

FIGURE 6: Cu sites of M150E *Af*NIR shown in the same orientation as in Figure 3. In panel A (top), an anomalous scattering difference map computed using data collected with λ = 1.3772 Å is contoured at 3σ, and panel B (bottom) is the same map computed using data with λ = 1.040 Å. In both maps, there is a large peak at the type II site whereas at the type I site a large anomalous difference is only detected at the shorter wavelength.

Crystal Contacts. The $P2_12_12_1$ crystal form has the lowest solvent content (V_m = 2.2 Å^3 mol/g) compared to the $P2_1$ (V_m = 2.4 Å^3 mol/g) and *R*3 (V_m = 2.8 Å^3 mol/g) forms (Matthews, 1968). A total of 107 residues (11%) are within 4 Å of residues of neighboring molecules in the native crystal (space group $P2_12_12_1$) and are defined as involved in crystal packing interactions. In contrast, the mutant crystals (space groups *R*3 and $P2_1$) have only 4% of the residues forming

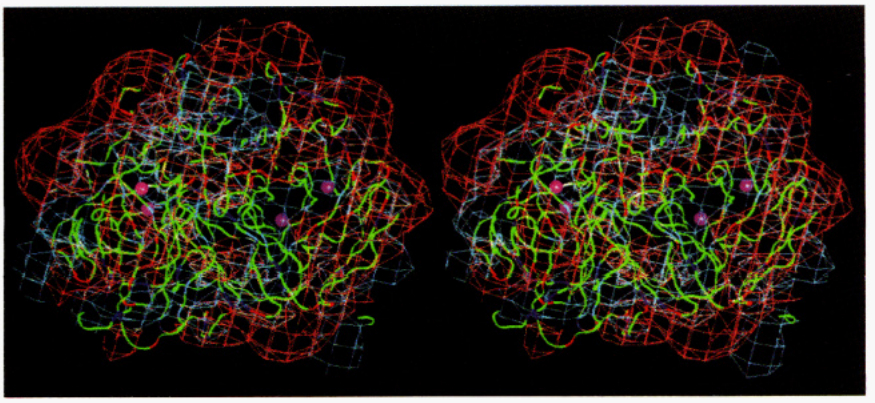

FIGURE 7: Electrostatic field surrounding *Af*NIR. The structure of *Af*NIR (green) is represented as a ribbon in the same orientation as in Figure 3. The positive (blue) and negative (red) electrostatic fields are contoured at $0.5kT/e$. Sections of the ribbon representing residues with full positive and negative charges are colored blue and red, respectively. The active site pocket leading to the type II Cu (purple) is positively charged. The region immediately surrounding the channel opening is negatively charged, including the proposed pseudoazurin binding site.

crystal contacts. Residues Glu8 and Asn65 form the majority of crystal contacts in the *R*3 crystal form. A similar interaction also occurs in the $P2_1$ form, which may explain why the amino terminus is more ordered in these crystals than in the native protein.

DISCUSSION

Fold of NIR. All of the domains containing a type I (blue) Cu site of known three-dimensional structure have a Greek key β-barrel fold (Adman, 1991). Both domains of NIR also possess this fold, suggesting that they share a common ancestor. The Cα atoms of the core 82 residues[3] of each domain were superimposed with an rms deviation of 1.01 Å. These core residues are related by a pseudo-2-fold symmetry axis (177.8° rotation, 0.22 Å translation) passing through the active site between subunits. This axis makes a 20° angle to the trimer axis. The sequence identity between equivalent residues of the two cores is 12%. All of the ligands for both Cu sites except for His145 are included in the core residue group. Active site residues Asp98 and His255 are related by the pseudo-2-fold axis as are the Cu ligand His100 and Ile257 (which forms part of the hydrophobic pocket). A helical loop containing three type I ligands, Cys136, His145, and Met150 in NIR, is found in all type I domains. In the C-terminal domain the fold of this loop is modified such that the Glu310 side chain can form part of the 3-fold channel, resulting in the Cα of His145 not being located in an equivalent position, excluding this residue from the overlap calculation. Three residues that form the trimer channel, Asp251, Arg253, and Phe282, are part of the core domain structure, and their counterparts in the N-terminal domain are 94, 96, and 113. The function of the channel along the trimer axis is not apparent. Residue Phe282 is a leucine in the *A. cycloclastes* structure and does not completely block the channel at the midpoint (Godden et al., 1991).

Role of the Copper Sites. Several studies have delineated the role of the two Cu sites in NIR. The structure of *Ac*NIR revealed that only the type II site is solvent exposed and that soaking NO_2^- into the crystals displaced the O ligand (water 503) at the type II site (Godden et al., 1991; Adman et al., 1995). EPR spectra and functional assays of *Ac*NIR with varying amounts of type II Cu present showed that the type II metal is required for NO_2^- reduction (Libby & Averill, 1992). Site-directed mutagenesis, combined with spectroscopic, functional, and initial crystallographic studies of the *A. faecalis* enzyme, clearly showed that the type I site receives an electron from pseudoazurin and that nitrite reduction occurs at the type II site (Kukimoto et al., 1994).

The Type I Site. Inspection of the NIR structure reveals that the surface near the type I ligand His145 is remarkably complementary to the proposed binding surface on pseudoazurin. In both NIR and pseudoazurin, the histidine ligand is associated with a hydrophobic patch. In the case of NIR this patch is surrounded by a ring of glutamic acid residues whereas in pseudoazurin a ring of lysine residues is present (Kukimoto et al., 1995). The proposed binding site for pseudoazurin is close to the opening of the active site pocket but does not occlude it.

The electrostatic field surrounding NIR was computed with the program DELPHI (Gilson et al., 1987). The computed field near the active site channel is illustrated in Figure 7. The most prominent feature is a strong negative field generated by the ring of negative charges at the surface near the type I site. The molecular surface is generally negatively charged except for the active site channel which possesses a positive field. Such a field would assist in directing the negatively charged substrate into the active site channel and have no effect on the neutral product. Protons required for the reaction may be inhibited by the field or may enter the active site by an alternate route such as via the chain of buried water molecules connected to His260.

The Type II Site. The geometry of the type II site of nitrite reductase is unique. No other protein of known structure possesses a metal site with a Cu atom coordinated by the Nε atoms of three histidines and water. The structurally most similar Cu site is found in ascorbate oxidase, where a similar arrangement of histidine ligands is observed but as part of a trinuclear site (type III) (Messerschmidt et al., 1989; Adman, 1991). The type II Cu site in superoxide dismutase (SOD) is liganded by four histidine side chains, one of which binds via the Nδ atom, in a tetrahedrally distorted square-planar geometry (Tainer et al., 1983). A water molecule is located

[3] The common core consists of residues 38−48, 60−69, 72−88, 94−100, 113−137, and 147−158 of the N-terminal domain and residues 173−183, 216−225, 232−248, 251−257, 282−306, and 313−324 of the C-terminal domain.

3 Å from the Cu site in SOD whereas in NIR a water or hydroxyl is directly liganded to the Cu site.

The histidine ligands of the type II site form extensive hydrogen bonds to the remainder of the structure. The hydrogen bond between His100 Nδ1 of one monomer and Glu279 Oε of another is notable in that a similar interaction occurs in other metalloenzymes. A conserved buried aspartic acid (Asp122) in SOD is hydrogen bonded to one of the Cu ligands (Tainer et al., 1982) and was shown to be required for enzyme function by site-directed mutagenesis (Getzoff et al., 1989). In the proteases thermolysin and carboxypeptidase, a similar carboxylate−imidazole ligand interaction is proposed to have an electron-donating effect thereby reducing the pK_a of a water molecule bound to the Zn site (Argos et al., 1978). By analogy, the Glu279 Oε−His100 Nδ1 hydrogen bond may also be critical for the function of NIR. Glu279 is also hydrogen bonded to the conserved residue Lys269 of the first monomer, giving rise to an altered + − + charge interaction, all completely buried.

The observation of a water or hydroxyl ligand at the type II site is confirmed by ENDOR spectroscopy on the related NIR from *Alcaligenes xylosoxidans*. This study showed that the apical position is occupied by a water molecule or hydroxide ion which is displaced upon addition of NO_2^- (Howes et al., 1994). The ENDOR study provided a Cu−water H distance of 2.9 (3) Å, which is compatible with the X-ray structures described here. The ENDOR work also suggests that when the substrate binds to the Cu, a proton is about 3.5 Å from the Cu center. This proton is not in either of the apical or planar positions but some intermediate position and is suggested to come from an imidazole ligand. No nitrogen coupling is observed using ^{14}N or ^{15}N, which is consistent with the substrate binding to the apical position where weak coupling is expected (Howes et al., 1994). Difference density maps of *Ac*NIR soaked with nitrite show density interpretable as nitrite bound asymmetrically via the oxygen atoms to the type II site, although not fully occupied (Godden et al., 1991; Adman et al., 1995).

The unaccounted for difference density at the type II site of native *Af*NIR (Figure 5) may result from the binding of azide present in the crystallization media. The literature in the interaction between azide and NIR is ambiguous. Azide has been shown to be an inhibitor of *Ac*NIR (Hulse & Averill, 1989) (and in unpublished EXAFS studies; R. Korzun, personal communications) but not of the *A. faecalis* enzyme (Kakutani et al., 1981a). The lack of extraneous density in the azide-free recombinant crystals does suggest that azide binds to the Cu atom in *Af*NIR.

M150E AfNIR. Atomic absorption spectroscopy of the M150E mutant has indicated the presence of only three Cu atoms per trimer and suggested that the mutation had destroyed the Cu binding site (Kukimoto et al., 1994). Furthermore, EPR spectroscopy no longer showed a distinct type I Cu signal as observed in the recombinant wild-type protein. Visible spectra lacked the 460, 590, and 700 nm peaks characteristic of type I Cu sites, and the crystals were not green. Thus, the presence of a large electron density peak at the type I site was unexpected. The structure unequivocally shows that a metal with at least a similar number of electrons as Cu is bound at the type I site.

Several metals have been substituted for Cu in the cupredoxin family both *in vitro* and *in vivo*. Engeseth and McMillin (1986) have shown that apoazurin can take up Ni, Co, and Mn. The structures of Cd-substituted azurin from *Alcaligenes denitrificans* (Blackwell et al., 1994) and Hg-substituted plastocyanin (Church et al., 1986) have been determined. When azurin from *Pseudomonas aeruginosa* was expressed in *E. coli,* a colorless inactive form was isolated and shown to be Zn substituted (Nar et al., 1992). In the structure of zinc azurin, a Zn−O bond of 2.3 Å was formed to the carbonyl oxygen of Gly45 and the Zn−Sγ distance is 2.30 Å, while the Zn−Nδ distances are 2.01 and 2.07 Å. The Zn is only 0.15 Å from the plane of the three strong ligands (His, Cys, His) as compared to 0.70 Å for M150E *Af*NIR. A Zn atom in the type I site of M150E *Af*NIR would be expected to possess the spectroscopic properties previously described (Kukimoto et al., 1994). Carboxylates have been observed to be ligands to the zinc proteases thermolysin and carboxypeptidase but have not been observed in the native forms of any Cu protein. The effective cation radius of Zn (0.71 Å) is very near that of Cu (0.69 Å) (Glusker, 1991), and any change in ligand bond lengths would not be observable in the crystal structure of M150E at the current resolution of 2.3 Å. Zn complexes and Zn proteins are commonly observed with four ligands in a tetrahedral arrangement like the type I site of NIR (Glusker, 1991).

Anomalous scattering was used to distinguish between Cu and Zn in M150E *Af*NIR. The anomalous scattering difference maps confirmed the hypothesis that M150E *Af*NIR possesses Cu at the type II site and Zn at the type I site as a result of the mutation (Figure 6). It is interesting to note that even though Zn was available to bind at the type I site, no Zn is detected at the type II site, suggesting a strong preference for Cu. No large changes in the geometry of the histidine and cysteine ligands at the type I site are required to accommodate the Zn atom. The replacement of the Met150 Sδ atom by the carboxylate oxygen of Glu150 is sufficient to alter the specificity of the type I site for Zn in the periplasm of *E. coli*. The replacement of Cu by a non-redox-active metal must be responsible for the greatly reduced electron-transfer efficiency with pseudoazurin (Kukimoto et al., 1994). At a wavelength of 1.377 Å, the anomalous signal from a fully occupied Zn (Table 5) would be sufficient to generate the small peak observed at the type I site (Figure 6A). However, the anomalous scattering experiment does not exclude the possibility of trace Cu present at the type I site. Any electron-transfer activity could be due to partial occupancy by Cu not detected by the anomalous scattering experiments.

The type I site methionine (Met121) of azurin from *P. aeruginosa* (analogous to M150E in NIR) has been mutated to all other amino acids (Karlsson et al., 1991). At pH 4, all of the mutants, including M121E, displayed EPR and optical spectroscopic characteristics of a type I Cu site. However, at neutral pH, the M121E and M121K replacements no longer display type I spectra. The transition in M121E azurin occurs at a pK of 4.9, and a new absorption band at 570 nm appears. The properties of this mutant have been explained by a pH-dependent change in the kind of Cu present at the type I site, although an X-ray structure has not yet been published. The blue Cu to protein ratio of the M121E mutant, as determined by EPR and absorption spectroscopy, was 0.19 as compared to 0.51 for the wild-type recombinant protein. Thus, in contrast to M150E *Af*NIR, the expression of M121E azurin in *E. coli* results in

the incorporation of low but significant amounts of Cu relative to the wild-type protein. The overall low copper contents of the expressed wild-type and mutant azurins and our results suggest that the type I site could be partially occupied by Zn which would not be detectable by EPR or absorption spectroscopy.

The structure of the M121Q mutant of azurin from *A. denitrificans* has been determined by X-ray analysis to 1.9 Å resolution (Romero et al., 1993). The protein used in this study was refolded in the presence of Cu to eliminate the presence of colorless (Zn) azurin; however, apo-M151Q azurin was shown to have the same selectivity for Cu over Zn as the wild-type protein. The crystal structure shows that the glutamine side chain interacts with the metal only via the Oϵ atom. The Cu Oϵ ligand bond length of 2.27 Å (average of two molecules in the asymmetric unit) is considerably longer than the 1.98 Å Zn Oϵ distance observed for M150E *Af*NIR, which is consistent with the preference of Zn for O ligands. The side-chain conformation in M151Q azurin does not follow that of the replaced methionine side chain, so the Oϵ atom lies closer to the position of the Sδ atom. The resulting Cu coordination is more similar to the wild-type azurin than that observed in the M150E mutant of NIR.

Conclusions. We have established that there is no difference between authentic wild-type *Af*NIR and its recombinant form. We have also shown that when a glutamate replaces the methionine ligand in a type I site, not only does the site remain without solvent but a Zn atom will bind instead of a Cu atom. The 2.0, 2.25, and 2.3 Å refinements of the native, recombinant, and M150E mutant structures, respectively, reconfirm the importance of His255 and Asp98 residues in the active site pocket, as expected from the overall similarity to the AcNIR structure. The AfNIR structure also shows that His260 and a chain of water molecules provide a path for protons required for the reduction of nitrite. Comparison of the specific interaction between Glu279 with His100 and Lys269 (all conserved) with similar interactions in other metalloenzymes provides strong evidence that these residues are important in creating the required copper ligand environment for catalysis.

There is a well-defined twofold relationship between more than half of the residues of each domain forming the active site. The molecular surface nearest the type I site contains negatively charged residues consistent with a docking site for the positively charged face of the electron-transfer partner of NIR, pseudoazurin. Calculation of the electrostatic potential surface shows that the site to which nitrite should be targeted is more positively charged than its surround.

The finding of a Zn atom at the type I copper site in the mutant protein, while a copper site remains at the type II site, not only explains the nonreducibility of the mutant NIR by pseudoazurin (still consistent with the hypothesis that the reducing electron goes through the type I site first) but also demonstrates the selectivity of the type II site for copper, even when Zn is present. This finding also demonstrates the importance of obtaining a molecular structure when interpreting the results of mutagenesis experiments.

ACKNOWLEDGMENT

Dr. Sakabe kindly provided access to beamline 6A at the KEK Photon Factory. Kohki Ishikawa (Ajinomoto Co.), Nobuya Nagashima (Ajinomoto Co.), Toshio Ichikawa (Kikkoman Co.), and members of Prof. Tanokura's laboratory provided valuable assistance with data collection at the Photon Factory. The authors thank Ethan Merritt for helpful discussions on the anomalous scattering experiments and are grateful to Ron Stenkamp for critically reading the manuscript.

REFERENCES

Adman, E. T. (1991) *Adv. Protein Chem. 42*, 145−197.
Adman, E. T., & Turley, S. (1993) in *Bioinorganic Chemistry of Copper* (Karlin, K. D., & Tyeklár) pp 397−405, Chapman & Hall, New York, NY.
Adman, E. T., Godden, J. W., & Turley, S. (1995) *J. Biol. Chem.* (in press).
Argos, P., Garavito, R. M., Eventoff, W., Rossmann, M. G., & Brändén, C. I. (1978) *J. Mol. Biol. 126*, 141−158.
Baker, E. N. (1988) *J. Mol. Biol. 120*, 1071−1095.
Blackwell, K. A., Anderson, B. F., & Baker, E. N. (1994) *Acta Crystallogr. D50*, 263−270.
Brünger, A. T. (1990) *X-PLOR, Version 3.1*, Yale University, New Haven, CT.
Brünger, A. T. (1992) *Nature (London) 355*, 472−475.
Chakrabarti, P. (1990) *Protein Eng. 4*, 49−56.
Church, W. B., Guss, J. M., Potter, J. J., & Freeman, H. C. (1986) *J. Biol. Chem. 261*, 234−237.
Collaborative Computational Project, Number 4 (1994) *Acta Crystallogr. D50*, 760−763.
Connolly, M. (1983) *Science 221*, 709−713.
Einspahr, H., Suguna, K., Suddath, F. L., Ellis, G., Helliwell, J. R., & Papiz, M. Z. (1985) *Acta Crystallogr. B41*, 336−41.
Engeseth, H. R., & McMillin, D. R. (1986) *Biochemistry 25*, 2448−2455.
Engh, R. A., & Huber, R. (1991) *Acta Crystallogr. A47*, 392−400.
Fenderson, F. F., Kumar, S., Liu, M.-Y., Payne, W. J., & LeGall, J. (1991) *Biochemistry 30*, 7180−7185.
Getzoff, E. D., Tainer, J. A., Stempien, M. A., Bell, G. I., & Hallewell, R. A. (1989) *Proteins: Struct., Funct., Genet. 5*, 322−336.
Gilson, M. K., Sharp, K. A., & Honig, B. H. (1987) *J. Comput. Chem. 9*, 327−335.
Glusker, J. P. (1991) *Adv. Protein Chem. 42*, 1−76.
Godden, J. W., Turley, S., Teller, D. C., Adman, E. T., Liu, M. Y., Payne, W. J., & LeGall, J. (1991) *Science 253*, 438−442.
Higashi, T. (1990) *J. Appl. Crystallogr. 23*, 253−257.
Howard, A. J., Gilliland, G. L., Finzel, B. C., Poulos, T. L., Ohlendorf, D. H., & Salemme, F. R. (1987) *J. Appl. Crystallogr. 20*, 383−387.
Howes, B. D., Abraham, Z. H. L., Lowe, D. J., Brüuser, T., Eady, R. R., & Smith, B. E. (1994) *Biochemistry 33*, 3171−3177.
Hulse, C. L., & Averill, B. A. (1989) *J. Am. Chem. Soc. 111*, 2322−2323.
Iwasaki, Y., Takeuchi, T., Tamiya, E., Karube, I., Nishiyama, M., Horinouchi, S., Beppu, T., Kadoi, H., Uchiyama, S., Suzuki, S., & Suzuki, M. (1992) *Electroanalysis 4*, 771−776.
Jones, T. A., Zou, J.-Y., Cowan, S. W., & Kjeldgaard, M. (1991) *Acta Crystallogr. A47*, 110−119.
Kakutani, T., Watanabe, H., Arima, K., & Beppu, T. (1981a) *J. Biochem. 89*, 463−472.
Kakutani, T., Watanabe, H., Arima, K., & Beppu, T. (1981b) *J. Biochem. 89*, 453−461.
Karlsson, B. G., Nordling, M., Pascher, T., Tsai, L.-C., Sjölin, L., & Lunberg, L. (1991) *Protein Eng. 4*, 343−349.
Kleywegt, G. J., & Jones, T. A. (1994) *Acta Crystallogr. D50*, 178−185.
Kraulis, P. (1991) *J. Appl. Crystallogr. 24*, 946−950.
Kukimoto, M., Nishiyama, M., Murphy, M. E. P., Turley, S., Adman, E. T., Horinouchi, S., & Beppu, T. (1994) *Biochemistry 33*, 5246−5252.
Kukimoto, M., Nishiyama, M., Ohnuki, T., Turley, S., Adman, E., Horinouchi, S., & Beppu, T. (1995) *Protein Eng. 8*, 153−158.

Laskowski, R. A., MacArthur, M. W., Moss, D. S., & Thornton, J. M. (1993) *J. Appl. Crystallogr. 26*, 283−291.
Libby, E., & Averill, B. A. (1992) *Biochem. Biophys. Res. Commun. 187*, 1529−1535.
Luzzati, V. (1952) *Acta Crystallogr. 5*, 802−810.
Matthews, B. W. (1968) *J. Mol. Biol. 33*, 491−497.
Merritt, E. A., & Murphy, M. E. P. (1994) *Acta Crystallogr. D50*, 869−873.
Messerschmidt, A., Rossi, A., Ladenstein, R., Huber, R., Bolognesi, M., Gatti, G., Marchesini, A., Petruzzeli, R., & Finazzi-Agro, A. (1989) *J. Mol. Biol. 206*, 513−529.
Nar, H., Huber, R., Messerschimdt, A., Filippou, A. C., Barth, M., Jaquinod, M., van de Kamp, M., & Canters, G. W. (1992) *Eur. J. Biochem. 205*, 1123−1129.
Navaza, J. (1994) *Acta Crystallogr. A50*, 157−163.
Nishiyama, M., Suzuki, J., Kukimoto, M., Ohnuki, T., Horinouchi, S., & Beppu, T. (1993) *J. Gen. Microbiol. 139*, 725−733.
Romero, A., Hoitink, C. W. G., Nar, H., Huber, R., Messerschmidt, A., & Canters, G. W. (1993) *J. Mol. Biol. 229*, 1007−1021.
Tainer, J. A., Getzoff, E. D., Beem, B. K., Richardson, J. S., & Richardson, D. C. (1982) *J. Mol. Biol. 160*, 181−217.
Tainer, J. A., Getzoff, E. D., Richardson, J. S., & Richardson, D. C. (1983) *Nature (London) 306*, 284−287.
Turley, S., Adman, E. T., Sieker, L. C., Liu, M.-Y., Payne, W. J., & LeGall, J. (1988) *J. Mol. Biol. 200*, 417−419.

BI951270A